

# Impact of Nitrogen Injection on Pore Structure and Adsorption Capacity of High Volatility Bituminous Coal

Junqiang Kang, Xuehai Fu,\* Derek Elsworth, and Shun Liang



Cite This: *Energy Fuels* 2020, 34, 8216–8226



Read Online

ACCESS |

Metrics & More

Article Recommendations

**ABSTRACT:** Nitrogen is often injected into coalbed methane (CBM) reservoirs to enhance the recovery by maintaining reservoir pressure and elevating permeability. Its effectiveness as a stimulant relies on impacts to the pore structure and related adsorption capacity of the coal reservoir. We quantify these changes in high volatility bituminous coal from Xinjiang, China, in response to nitrogen injection. Changes in pore size distribution (PSD) were characterized by high-pressure mercury injection (HPMI), low-pressure nitrogen gas adsorption (LP-N<sub>2</sub>GA), and carbon dioxide gas adsorption (LP-CO<sub>2</sub>GA). Corresponding changes in post-treatment adsorption capacity were measured by low-field nuclear magnetic resonance (LF-NMR) and isothermal adsorption. The specific pore volume and surface area of macropores (>50 nm), mesopores (2–50 nm), and micropores (<2 nm) all increased following nitrogen injection, as did measured adsorption capacity. These observations are consistent with an increase in surface area and improved connection between macropores that were previously unconnected or poorly connected. Nitrogen was subsequently diffused into mesopores and micropores, and then adsorbed into the pore walls. Nitrogen adsorption decreases surface energy and develops internal stress by differential deformation of the different macerals, that destroys the connectivity of mesopores and micropores. The effect of nitrogen injection on specific pore volume, surface area, and adsorption capacity also differs for different material and reservoir conditions. Higher mineral content and even distribution of macerals may improve the effect of PSD and adsorption capacity change. The presence of water hinders both flow and adsorption of nitrogen, leaving the mesopores unaffected by nitrogen injection. Water has little effect on changes in micropore architecture as a result of nitrogen injection due to capillary exclusion.

## 1. INTRODUCTION

Enhancement of coalbed methane (CBM) recovery by gas injection is a favored method to maximize both gas production and environmental protection.<sup>1,2</sup> Nitrogen and carbon dioxide are the main injected gases. Although carbon dioxide injection can improve methane production<sup>2</sup> and also achieve geological storage of carbon dioxide,<sup>3</sup> its strong adsorption capacity and propensity for swelling may result in a permeability decrease that stanches production.<sup>2,4</sup> Therefore, carbon dioxide stimulation is more suitable for coal reservoirs with an initial high permeability. The adsorption capacity of nitrogen is approximately one-quarter that of carbon dioxide, results in concomitantly reduced swelling and permeability reduction, and is more suitable for coal reservoirs with initial low permeability.<sup>5,6</sup>

Compared with hydraulic fracturing to improve reservoir permeability and carbon dioxide injection to enhance CBM recovery by competitive adsorption with methane,<sup>2,4</sup> enhancing gas production by nitrogen injection results from both reducing methane adsorption partial pressure and improving reservoir fracture permeability.<sup>2,7</sup> However, the influence of nitrogen injection on pore size distribution (PSD) and adsorption capacity remains poorly understood. Nitrogen flooding works by injecting then maintaining high-pressure gas into the coal reservoir.<sup>2,7</sup> The injected gas not only interacts with methane to promote methane desorption but

also interacts with the coal reservoir, influencing pore connectivity, PSD, and adsorption capacity.

The influence of strongly sorbing carbon dioxide on the PSD of coal is well-known,<sup>8–11</sup> but the response to slightly sorbing gases is relatively less well-defined.<sup>5,12</sup> Comparing the PSD of semianthracite before and after nitrogen injection using high-pressure mercury injection (HPMI) showed increases in mesopores and macropores in the range 10–100 nm, macropores in the range 100–1000 nm, and macropores in the range greater than 1000 nm in proportions of 2.1%, 47.8%, and 141.0%, respectively.<sup>5</sup> Porosity and permeability also increased by 22.6% and 29.9%, respectively. Low-pressure pulsed air (78% nitrogen) injection on low volatility bituminous coal<sup>12</sup> resulted in the volume of mesopores in the range 7.2–10 nm decreasing by 17.95%, mesopores and macropores in the range 10–100 nm increasing by 25.85%, macropores in the range 100–100 nm increasing by 438.13%, and macropores in the range greater than 1000 nm increasing by 149.13%. Thus, laboratory experiments suggest that

Received: April 15, 2020

Revised: June 7, 2020

Published: June 15, 2020



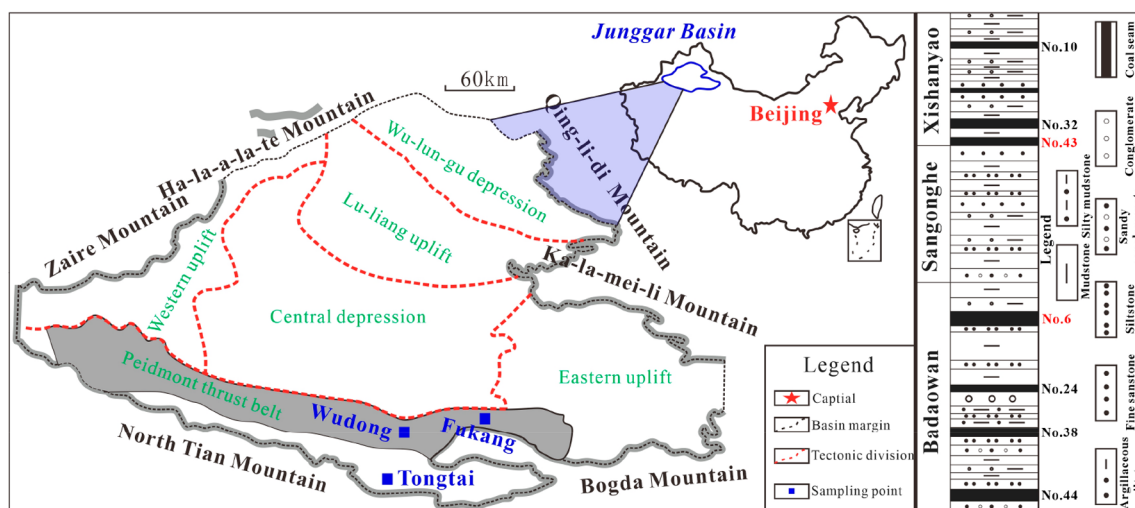


Figure 1. Structural geological map and stratigraphy together with sampling locations.

Table 1. Vitrinite Reflectance, Proximate Analysis, and Maceral Composition of FK, WD, and TT Samples

no.	location	$R_{o,max}/\%$	$M_{ad}/\%$	$A_d/\%$	$V_{daf}/\%$	vitrinite/%	inertinite/%	liptinite/%
FK	Fukang	0.64	2.77	2.74	39.64	79.80	18.7	0.60
WD	Wudong	0.72	2.53	4.12	32.24	34.20	62.20	3.60
TT	Tongtai	0.34	3.12	4.95	31.42	18.58	79.78	1.64

nitrogen injection can both improve pore connectivity and increase permeability. Field injection experiments on 34 low-ranking CBM wells in the Fruit and Formation, San Juan Basin, USA, resulted in a 5-fold increase in the total productivity and an increase in the recovery factor of 10–20%.<sup>1</sup> CO<sub>2</sub> injection into high volatility bituminous coal in the Ishikari coalfield, Japan, identified only slow infiltration before preconditioning with nitrogen injection.<sup>2</sup> After nitrogen injection, the injection rate of CO<sub>2</sub> increased by 60% after 15 days—potentially resulting from the improved connectivity of existing fractures.

However, previous studies are not conclusive regarding the potential for improvement in productivity and in probing relevant mechanisms. These observations<sup>5,12</sup> neglect high volatility bituminous coal—probing by HPMI cannot effectively characterize changes in the macropore and transition pore (>100 nm) architecture. Similarly, the connectivity between pores affects both the desorption and the migration of methane and has an important impact on gas production.<sup>13,14</sup> Changes in the smaller diameter pores after nitrogen injection also affect the adsorption capacity of the coal reservoir. There are many test methods for pore size distribution and adsorption capacity,<sup>15–17</sup> but the characterization methods in coal have their own advantages. HPMI can accurately characterize macropores, but not micropores and mesopores.<sup>16</sup> However, low-pressure nitrogen gas adsorption (LP-N<sub>2</sub>GA) and by carbon dioxide gas adsorption (LP-CO<sub>2</sub>GA) can effectively characterize mesopores and micropores.<sup>16,17</sup> Conventional isothermal adsorption, such as volumetric method and gravimetric method, can accurately characterize the adsorption capacity of coal samples, but it is unable to distinguish the differences of adsorption capacity of different pore sizes.<sup>16,18</sup> Moreover, the samples needed for conventional isothermal adsorption must be powder samples, and stress cannot be applied to restore the real formation. This is the advantage of LF-NMR; that is, it can apply stress, does

not destroy the sample, and distinguishes the adsorption capacity of different pore sizes.<sup>15,19</sup>

We address these shortcomings by exploring the characteristics of highly volatile bituminous coal from the southern margin of the Junggar basin, Xinjiang, China, to explore changes in PSD and related adsorption capacity as a result of nitrogen injection. Both intact and powdered samples, each dried and then at equilibrium moisture content (wetted), were used to explore the impacts of scale and moisture content on PSD and adsorption capacity. Changes in PSDs resulting from nitrogen flooding were measured by HPMI, LP-N<sub>2</sub>GA, and LP-CO<sub>2</sub>GA. These measured changes in pore architecture were then correlated with observed changes in methane adsorption capacity recovered from isothermal adsorption and low field nuclear magnetic resonance (LF-NMR) to define mechanistic linkages.

## 2. MATERIALS AND METHODS

The three high volatility bituminous coals were used both intact and powdered and prepared under two conditions of water saturation. These samples were subject to nitrogen flooding and changes in pore-scale architecture measured, together with its impact on methane adsorption characteristics.

**2.1. Sample Collection and Preparation.** The samples were recovered from the No. 6 coal seam of the Badaowan Formation of the Fukang (FK) coal mine, the No. 43 coal seam of the Xishanyao Formation of the Wudong (WD) coal mine, and the No. 24 coal seam of the Xishanyao Formation of the Tongtai (TT) coal mine (Figure 1). The samples were immediately sealed upon collection to prevent oxidation and water loss. The samples were prepared in two conditions—intact core and powdered and as both dry and at equilibrium water content. Three cylindrical core samples (25 × 50 mm) were cored parallel to bedding (FK (1 sample) and WD (2 samples)) and one sample powdered (TT) to 60–80 mesh.<sup>17,18</sup>

Proximate analysis was completed according to ISO 17246-2005<sup>20</sup> and vitrinite reflectance ( $R_{o,max}$ ) and maceral composition determined according to ISO 7404-5-2009.<sup>21</sup> The results show that the three coal samples were all high volatility bituminous coals with insignificant

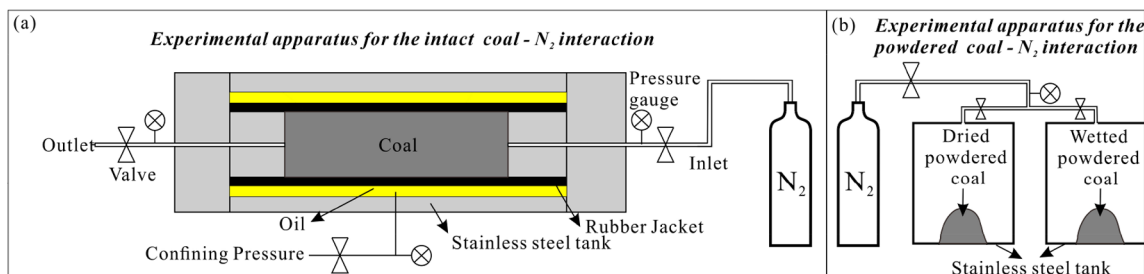


Figure 2. Schematic of nitrogen injection experiments: (a) for intact samples; (b) for powdered samples.

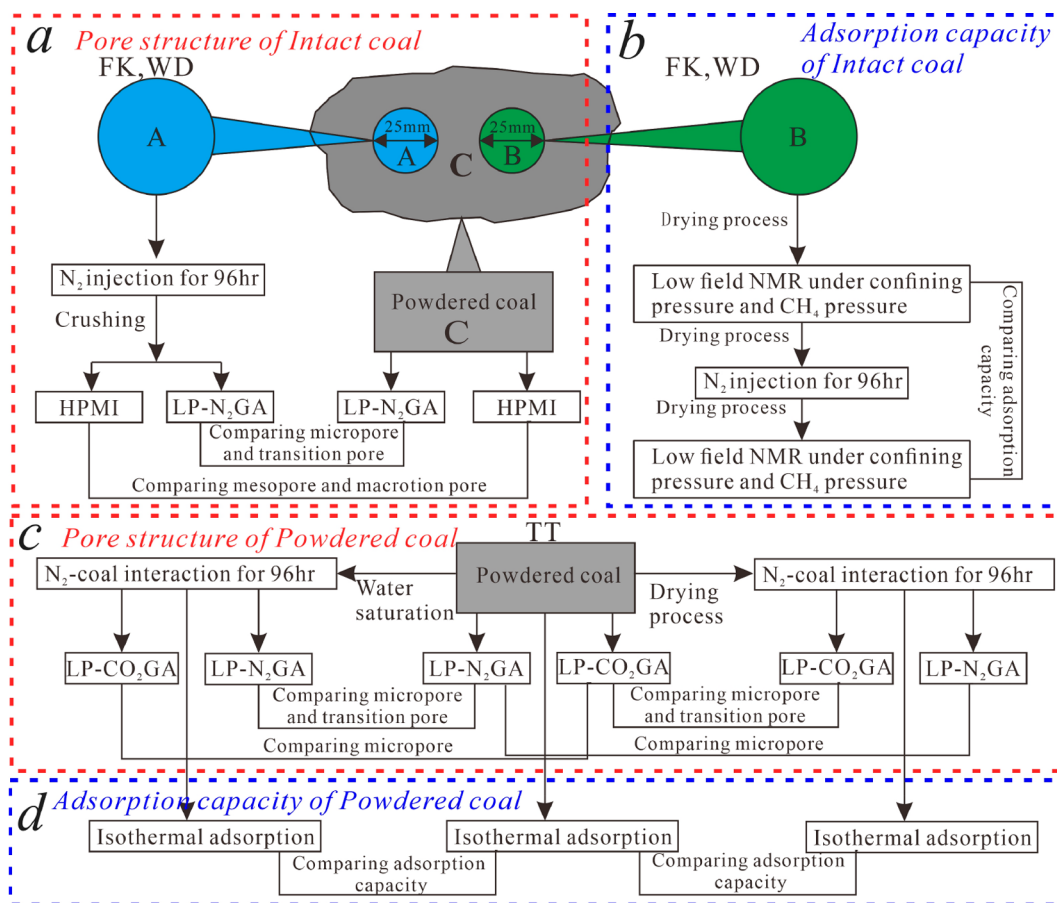


Figure 3. Experimental workflow for nitrogen injection.

differences in volatile ( $V_{\text{daf}}$ ), ash ( $A_{\text{d}}$ ), and water contents ( $M_{\text{ad}}$ ). One possible exception was that the FK had a high vitrinite content and WD and TT high inertinite contents (Table 1).

**2.2. Experimental Procedures.** **2.2.1. Pore Architecture Measurements.** The intact cylindrical samples were enclosed in a core holder and injected with nitrogen at 5 MPa (Figure 2a) at the upstream, discharging to 0.1 MPa (atmospheric pressure) downstream, and under a confining pressure of 10 MPa base on comprehensive burial depth 400–500 m of samples collected. The confining pressure is applied to make the experimental environment more in line with the real reservoir conditions. Once stable gas flow was established at the outlet, the downstream valve was closed to simulate shut-in.<sup>2</sup> The samples were then removed after 96 h and split into two fractions for HPMI and LP-N<sub>2</sub>GA tests, respectively. HPMI was used to characterize the PSD larger than 50 nm, LP-N<sub>2</sub>GA for pores in the range 2–30 nm and LP-CO<sub>2</sub>GA for pores smaller than 2 nm.<sup>16,22</sup> HPMI measurements were made with a Micromeritics Autocore IV 9500 instrument with samples crushed to 2 mesh.<sup>9</sup> LP-N<sub>2</sub>GA measurements were made with a Micromeritics Tristar II 3020

specific surface area analyzer with samples crushed to 60 mesh.<sup>17</sup> The samples close to the sampling point of intact cylindrical samples were also tested for HPMI and LP-N<sub>2</sub>GA. These data are considered representative of the pore architecture before nitrogen flooding as the sampling locations are close.<sup>5,11,12</sup>

The powdered samples were obtained by first crushing to 60 mesh then dividing into three fractions. The first fraction was retained as control and not subjected to nitrogen injection. Before the experiment, the sample needs to be dried at a low temperature to eliminate residual moisture in the sample, so we chose 60 °C to dry the sample, because the drying process at this temperature will not affect the pore structure of the sample.<sup>23–25</sup> The second fraction was dried at 60 °C for 6 h and then saturated in K<sub>2</sub>SO<sub>4</sub> solution for 48 h as a wetted sample. The third fraction was dried at 60 °C for 6 h and retained as a dried sample. Because the two high-pressure stainless steel cells were controlled by separate valves, moisture could not enter the other experimental chamber and affect the results. The two powdered samples were placed into a high-pressure stainless steel cell and injected with nitrogen to 5 MPa (Figure 2b). Following this, all

three samples were dried for 5 h at 60 °C before being characterized for PSD by LP-N<sub>2</sub>GA and LP-CO<sub>2</sub>GA. HPMI measurements of PSD were excluded since the particle size was much smaller than the required 2 mesh.

**2.2.2. Adsorption Capacity Measurements.** Conventional isothermal adsorption measurements were not completed on the intact cylindrical samples due to their low mass (~32 g)<sup>26</sup>—LF-NMR was used as an alternative. LF-NMR was used to measure both the overall adsorption capacity and the capacity in different pore size ranges.<sup>27,28</sup> A MacroMR12-150H-I LF-NMR tester (Suzhou Niumag Analytical Instrument Co.) was used<sup>6</sup> on sample WD. The sample was placed in the core holder of the LF-NMR instrument, purged of gas impurities before being saturated with methane to 5 MPa at a confining pressure of 10 MPa.<sup>28</sup> After methane saturation, that is, the LF-NMR data no longer changed with time, the sample was removed and dried at 60 °C for 5 h to remove the methane, cooled to 25 °C before replacing into the core holder, and injected with nitrogen at 5 MPa (10 MPa confining pressure) until it was discharged from the downstream and shut in for 96 h. Following the shut-in, the sample was dried at 60 °C for 5 h to remove the nitrogen. After again cooling to 25 °C, the sample was returned to the core holder and saturated with methane and the change in sorption measured from the change in the peak in the NMR spectrum from both before and after nitrogen injection.

The change in methane sorption capacity before to after nitrogen injection was measured on the powdered sample using a TerraTek Isotherm Measurement System (IS-100) using the gravimetric method at a temperature of 25 °C.

The complete experimental workflow is shown in Figure 3.

### 3. RESULTS

Nitrogen injection potentially influences pore scale architecture and, through this, impacts methane adsorption capacity. We examine this suggestion by independently measuring changes in pore architecture across scales<sup>16,27</sup> and in comparing these observations with observed changes in methane adsorption capacity. The incremental rate of specific pore volume, specific surface area of different pore diameters, and adsorption capacity after nitrogen injection is

$$c = \frac{S - S_0}{S_0} \times 100\%$$

where  $c$  is incremental rate;  $S$  is value of specific parameters after nitrogen injection;  $S_0$  is value of specific parameters before nitrogen injection.

**3.1. Effect of Nitrogen Injection on PSD.** We examine the impact of nitrogen injection across the range of IUPAC pore size classifications. These are macropores (>50 nm), mesopores (2–50 nm), and micropores (<2 nm).

**3.1.1. Macropore Evolution—Dried Intact Samples Based on HPMI.** After nitrogen injection, the total specific pore volume and specific surface area of macropores in the dried intact FK and WD samples increased (Table 2). The total specific pore volume of FK increased by 120.75%, and that of

WD increased by 272.22%; the specific surface area of FK increased by 114.53%, and that of WD increased by 427.43%, indicating that the pore/fracture volume accessible to mercury increased after nitrogen injection—consistent with previous studies.<sup>5,12</sup> Compared with the increase in specific pore volume and specific surface area, the mercury removal efficiency decreased (Table 2). Thus, although more mercury enters the pores, it is difficult to recover, with this related to the newly formed pore structure. The mercury intrusion–extrusion relation shows that the lag ring increases after nitrogen injection (Figure 4), suggesting the generation of more ink bottle pores.<sup>16</sup>

The specific pore volume in the pore size ranges 30 000–1 000 000 nm and 50–300 nm was significantly increased for sample FK—although there was no significant change in the pore size range 300–30 000 nm. However, the specific pore volume in the pore size range 50–3000 nm for sample WD increased significantly following nitrogen injection but with insignificant effect on the large pores in the range 3000–50 000 nm, and the specific pore volume is unchanged before and after nitrogen injection (Figure 5).

**3.1.2. Mesopore (2–50 nm) Evolution—Intact and Powdered Samples Based on LP-N<sub>2</sub>GA.** The specific pore volume of mesopores in the two dried intact samples (FK and WD) increased by 0.6% and 56.33% following nitrogen injection, respectively. The specific surface area of these mesopores increased by 21.43% and 72.41%, respectively. The specific pore volume of the dried and wetted powdered samples of TT increased by 106.38% and –5.08%, respectively, while the specific surface areas increased 80.00% and –2.86%, respectively (Table 3). Compared with the adsorption–desorption curve before and after nitrogen injection, adsorption volume increased together with accentuated hysteresis between injection and extrusion (Figure 6), suggesting pores open at both ends.<sup>29,30</sup>

Sample FK showed significant specific pore volume change in the larger mesopores (20–50 nm) with those in the lower range (2–20 nm) remaining unchanged (Figure 7a). The specific surface area shows similar variation characteristics with the changes of specific pore volume (Figure 7c). The specific pore volume and specific surface area of the 2–50 nm pores in sample WD were significantly increased (Figure 7b,d). The results for the powdered samples, both dried and wetted, following nitrogen injection, were different from those of the dried intact samples, showing that the smaller the initial pore size, the more obvious the increase (Figure 8a,b). The specific pore volume and specific surface area of the powdered sample TT changed most in the pore size range 2–7 nm and less in the range 7–30 nm (Figure 8a,b). The specific pore volume and specific surface area increased more in the dried powdered relative to that in the wetted sample (Figure 8).

**3.1.3. Micropore Evolution—Powdered Samples Based on LP-CO<sub>2</sub>GA.** After nitrogen injection, the specific pore volumes of both dried and wetted powdered samples increased by 48.23% and 58.66%, respectively, and the increase in specific surface area was 58.41% and 63.81%, respectively (Table 4). The adsorption capacity was significantly higher after nitrogen injection, but there was no significant difference between dried and wetted samples (Figure 9). The smaller pores increased in diameter the most. The increase in specific pore volume in the range 0.75–1.5 nm was small, while the change in the range 0.3–0.7 nm pores was large (Figure 10).

**Table 2. HPMI Data before and after Nitrogen Injection**

No.	total specific pore volume cm <sup>3</sup> /g	total pore area m <sup>2</sup> /g	mercury removal %
FK-Initial	0.0811	8.415	26.8
FK-After	0.0970	9.638	21.0
Increment	120.75%	114.53%	
WD-Initial	0.0644	1.243	36.5
WD-After	0.0782	5.313	27.6
Increment	272.22%	427.73%	

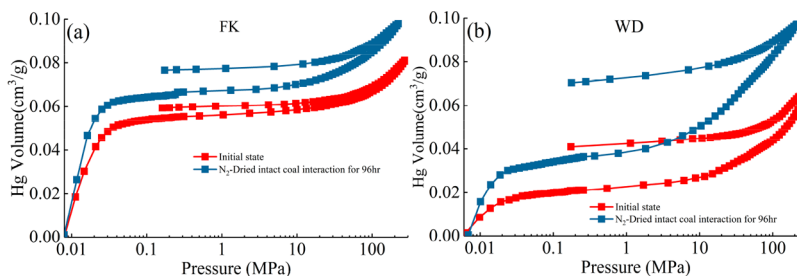


Figure 4. Observations of mercury intrusion–extrusion for dried intact samples FK and WD both before and after nitrogen injection.

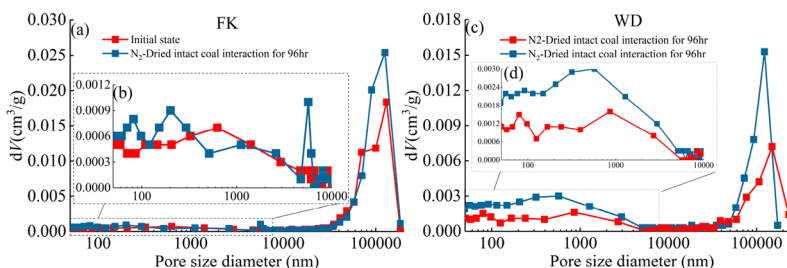


Figure 5. PSD of macropores of dried intact samples FK and WD before and after nitrogen injection: (a) and (c) specific pore volume for pores 50–100 000 nm; (b) and (d) specific pore volume for pores 50–10 000 nm.

Table 3. Specific Pore Volume and Specific Surface Area Data Based on LP-N<sub>2</sub>GA before and after Nitrogen Injection

no.	sample attribute	sample morphology	total area	total volume	variation after N <sub>2</sub> interaction for 96 h	
			m <sup>2</sup> /g	cm <sup>3</sup> /g	total area	total volume
FK	Initial state		0.1160	0.0014		
	N <sub>2</sub> interaction for 96 h	Dried intact sample	0.1167	0.0017	0.60	21.43
WD	Initial state		0.7713	0.0058		
	N <sub>2</sub> interaction for 96 h	Dried intact sample	1.2058	0.0100	56.33	72.41
TT	Initial state		1.9090	0.0035		
	N <sub>2</sub> interaction for 96 h	Dried powder sample	3.9398	0.0063	106.38	80.00
	N <sub>2</sub> interaction for 96 h	Wetted powder sample	1.8119	0.0034	−5.08	−2.86

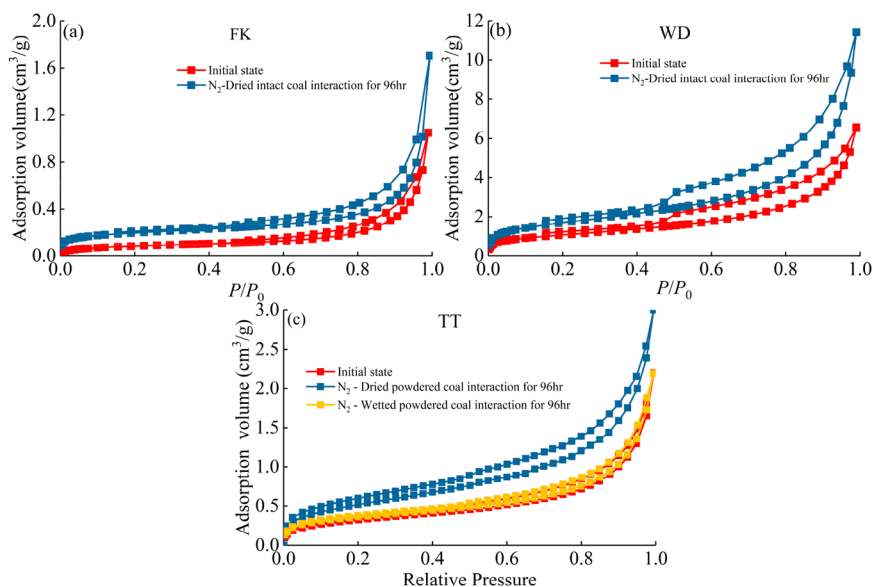
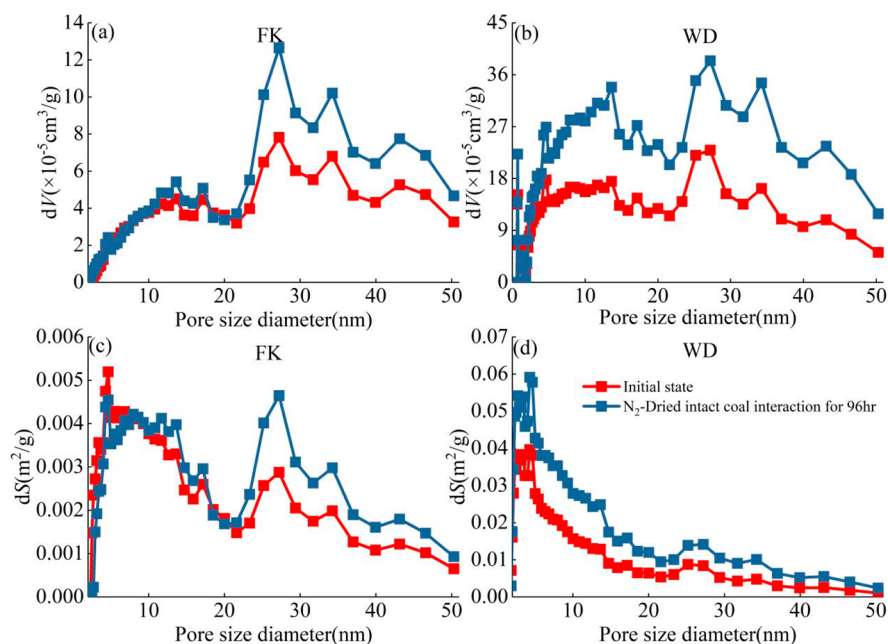


Figure 6. Adsorption–desorption curve of samples both before and after nitrogen injection: (a) and (b) dried intact coal; (c) dried and wetted powdered coal.

3.2. Effect of Nitrogen Injection on Adsorption Capacity. LF-NMR was used to characterize the adsorption

capacity of the intact sample, and isothermal adsorption by the gravimetric method was used for the powdered samples. LF-



**Figure 7.** PSD of mesopores of dried intact samples before and after nitrogen injection: (a) and (b) specific pore volume distribution of 2–25 nm; (c) and (d) specific surface area distribution of 2–50 nm.

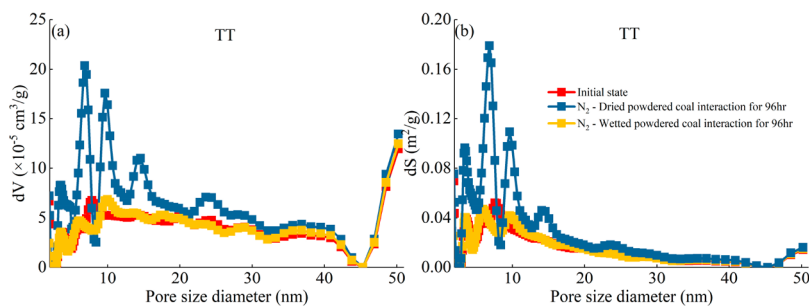


**Figure 8.** PSD of mesopores of powdered samples before and after nitrogen injection: (a) specific pore volume distribution of 2–25 nm; (b) specific surface area distribution of 2–25 nm.

**Table 4.** Specific Pore Volume and Surface Areas Recovered from LP-CO<sub>2</sub>GA before and after Nitrogen Injection

sample attribute	sample morphology	total area	total volume	variation after N <sub>2</sub> interaction for 96 h	
		m <sup>2</sup> /g	cm <sup>3</sup> /g	total area	total volume
Initial state		151.73	0.0479		
N <sub>2</sub> interaction for 96 h	Dried powder	240.35	0.0710	58.41	48.23
N <sub>2</sub> interaction for 96 h	Wetted powder	248.55	0.0760	63.81	58.66

NMR is used to characterize the distribution of pore and adsorption capacity of coal by the vibration of hydrogen atoms in a magnetic field.<sup>28,31,32</sup> Methane in coal will produce different relaxation due to different occurrence states, such as surface relaxation ( $T_{2S}$ ) of adsorbed methane and bulk relaxation ( $T_{2B}$ ) of free methane. Diffusion relaxation can be neglected in low magnetic field.<sup>28,32</sup> The relationship between relaxation time and relaxation time is as follows:

$$\frac{1}{T_2} = \frac{1}{T_{2B}} + \frac{1}{T_{2S}} + \frac{1}{T_{2D}} \approx \frac{3T_k}{298\eta} + \rho \left( \frac{S}{V} \right)_{\text{pore}}$$

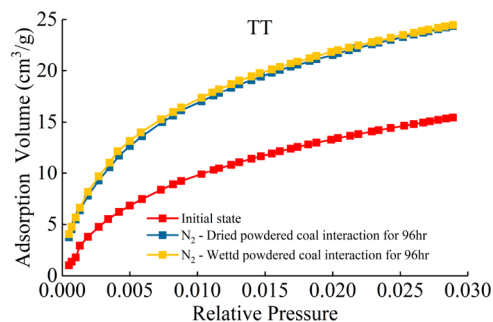


**Figure 9.** CO<sub>2</sub> adsorption curve of micropores before and after nitrogen injection.

where  $T_k$  is the ambient temperature (298 K) in K;  $\eta$  is the fluid viscosity in cp;  $\rho$  is the surface relaxation rate in m/s,  $S$  is the specific surface area of the pore in m<sup>2</sup>,  $V$  is the specific volume of the pore in m<sup>3</sup>. Based on this, the quantity and distribution of methane in coal can be measured.<sup>33</sup> The coal adsorption capacity measured by the conventional isothermal adsorption method and the LF-NMR method is comparable on the premise that the sample sizes of both are the same.<sup>27,28</sup> However, due to the purpose of the study, the sample size is

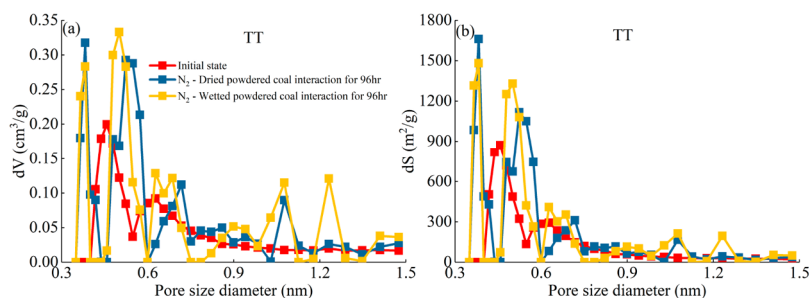


**Figure 10.** PSD of micropores for powdered samples before and after nitrogen injection: (a) specific pore volume distribution for pores in the range 0.3–1.5 nm; (b) specific surface area distribution for pores in the range 0.3–1.5 nm.

different, so here we will not compare the measurement results of LF-NMR and conventional isothermal adsorption methods, but only compare the measurement results before and after nitrogen injection under the same measurement method.

The results showed three peaks, P1, P2, and P3 in the  $T_2$  spectrum (Figure 11). According to the principle of LF-NMR,

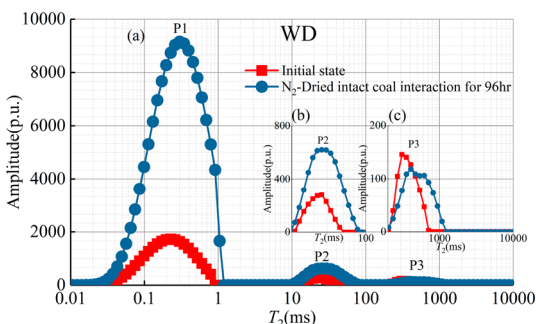


**Figure 11.** LF-NMR relaxation spectra for dried intact sample WD saturated with methane before and after nitrogen injection: (a) spectrum with a relaxation time of 0.01–2 ms, corresponding to adsorption pores in the range 0–100 nm; (b) spectrum with relaxation time of 10–100 ms, corresponding to the seepage pores in the range 100–10 000 nm; (c) spectrum with relaxation time of 200–10000 ms, corresponding to fractures with apertures in the range >10000 nm.

the P2 and P3 peaks represent free methane, while the relaxation of the P1 peak represents adsorbed methane.<sup>10,28</sup> The rise in the peak value means that more methane is absorbed or stored by the coal, consistent with an increase in specific surface area or specific pore volume.<sup>28</sup> The peak spectral area corresponds to the methane adsorption volume. The spectral area is obtained from the deconvolution integral of the peak spectrum.<sup>28</sup> The adsorbed methane increased by 467% following nitrogen injection; free methane increased by about 154% (Figure 12). The results show that nitrogen injection can significantly improve the methane adsorption capacity of coal. For coal reservoirs, adsorbed methane is mainly stored in micropores and mesopores, while free methane is mainly stored in macropores.<sup>17,33</sup> The changes of adsorbed methane and free methane also indicate that nitrogen injection can significantly change the increase of the specific surface area and specific pore volume of the pore; that is, the pore connectivity is enhanced.

The results for the dried and wetted powdered TT samples also show that the adsorption capacity determined by isothermal adsorption increases after nitrogen injection (Table 5, Figure 13). After nitrogen injection, the  $V_L$  increased

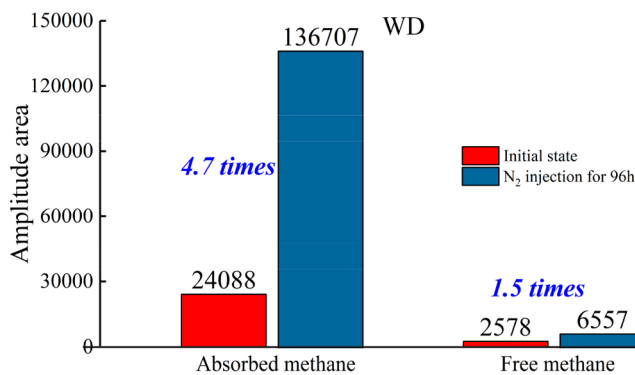


**Figure 12.** Spectral area increments of dried intact sample WD in adsorbed methane and free methane before and after nitrogen injection.

**Table 5. Spectral Area Change of Intact WD Coal Sample before and after Nitrogen Injection**

peak	P1	P2+P3
Methane phase	Absorbed methane	Free methane
Initial	24088	2578
N <sub>2</sub> - Dried intact interaction for 96 h	136707	6557
Change rate	467%	154%

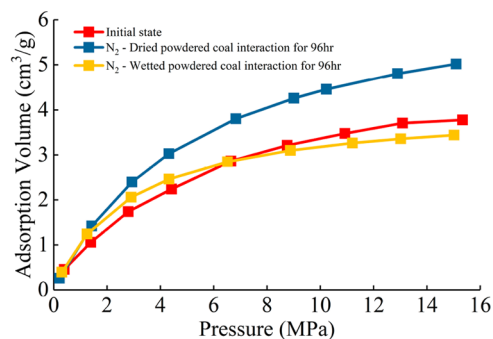


**Figure 13.** Isothermal adsorption curves of dried and wetted powdered sample TT before and after nitrogen injection.

by 30.90% after the dried sample was treated with nitrogen for 96 h (Table 6), while the  $V_L$  decreased by 21.30% after the wetted sample was treated with nitrogen. The  $P_L$  of the two samples decreased, with that of the wetted sample being the most obvious (47.82%). The slight decrease of the adsorption capacity of the wetted sample is probably due to the incomplete drying of the sample, which leads to a decrease in the adsorption capacity.

**Table 6.**  $V_L$  and  $P_L$  Increments of TT Sample before and after Nitrogen Injection

sample attribute	Langmuir volume	Langmuir pressure	Langmuir volume change rate/%
	cm <sup>3</sup> /g	MPa	
Initial state	5.21	5.52	
N <sub>2</sub> -Dried powder interaction for 96 h	6.82	5.41	30.90
N <sub>2</sub> -Wetted powder interaction for 96 h	4.10	2.88	-21.30

#### 4. DISCUSSION

The current results showed that nitrogen injection can effectively change the PSD and adsorption capacity of the studied coals (Figures 5, 8, 10, 12, and 13) together with fracture architecture.<sup>2,7</sup>

Pores and fractures in coal are often filled with minerals and powdered coal matrix, potentially reducing pore connectivity.<sup>34,35</sup> For macropores, pressurized nitrogen may break through between either unconnected macropores or those poorly connected due to presence of filler. The pressured gas will first connect the pores with the weakest barrier strength, forming a new narrow channel,<sup>7</sup> with this channel developing an ink bottle form with low mercury removal efficiency. The stress will affect the effect of nitrogen on fractures and macropores. Under higher stress, the closure is greater,<sup>36</sup> and the stress will increase the adhesion of matrix particles and minerals in fractures and macropores,<sup>37,38</sup> which requires higher nitrogen pressure, and longer time will increase the connectivity. For mesopores and micropores, carbon dioxide injection will often produce carbonic acid, dissolving minerals and organic matter in the coal.<sup>9,10,39</sup> Conversely, nitrogen does not form an acidic residue to dissolve minerals.<sup>2</sup> The effect of

nitrogen in coal is mainly to reduce surface energy of the coal matrix by gas adsorption and to change the internal stress due to adsorptive swelling of the different components.<sup>11,40,41</sup> The decrease in the surface energy decreases the bond strength and stress and may create a new channel to connect previously unconnected pores.<sup>40,41</sup> The different macerals and minerals present in the coal generate differential sorption/swelling stresses causing weak bonds to break and pores to connect.<sup>11</sup> Carbon dioxide injection will generally produce fractures,<sup>11</sup> but nitrogen adsorption is weaker and the severity of fracturing is less. Thus, for nitrogen injection, the change in connectivity of mesopores and micropores is caused by gas adsorption and damage rather than by gas overpressure.<sup>5,42</sup> Coal and fractures/pores as a whole, and the change of one kind of fractures/pores, will undoubtedly affect the connectivity of other kind of fractures/pores.<sup>4,29</sup> Undoubtedly, the change of connected specific pore volume and specific surface area affect the adsorption capacity of the reservoir (Figures 11, 12, and 13).<sup>13</sup>

Different samples show different results (Tables 2 and 3; Figures 5 and 7). The mineral content (ash yield) of sample WD was higher than that of sample FKs (Table 1). These minerals will fill the pores/fractures (Figure 14), accounting for the different changes observed for the macropores/fractures between WD and FK. The adsorption capacity of WD was higher than that for FK (Table 3; Figure 7c,d), which results in larger adsorption swelling.<sup>26</sup> There were three kinds of macerals in the WD samples, with the proportion of each maceral more uniform than that of FK, dominated by vitrinite. This will result in greater internal stresses due to differential deformations of the contrasting macerals than that in the FK samples. This in turn drives a larger specific pore volume and specific surface area increase. Compared with the specific pore volume and specific surface area increase of mesopores of the dried intact (FK and WD) and powdered (TT) sample, the

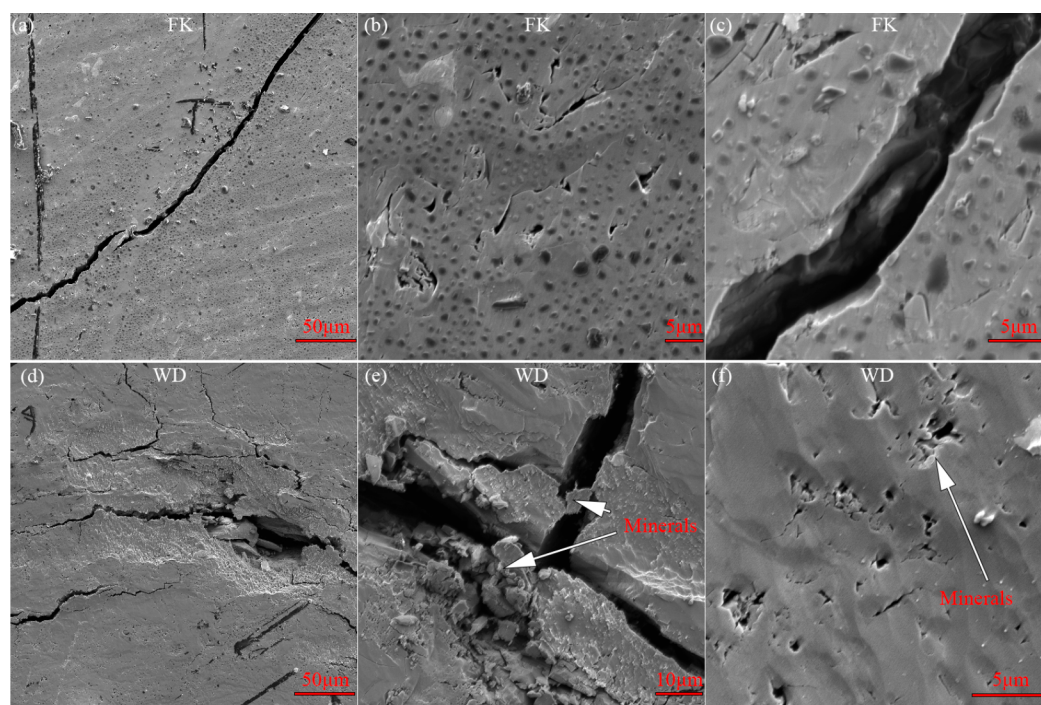


**Figure 14.** SEM pictures of samples FK and WD: (a) and (b) sample FK with less infilling within the fractures; (c) and (d) sample WD with infilling of minerals and powdered coal.

larger the initial specific surface area, the larger the increase after nitrogen injection, due to a larger adsorption deformation and internal stress (Table 3; Figure 15).<sup>11,41</sup> Water in the

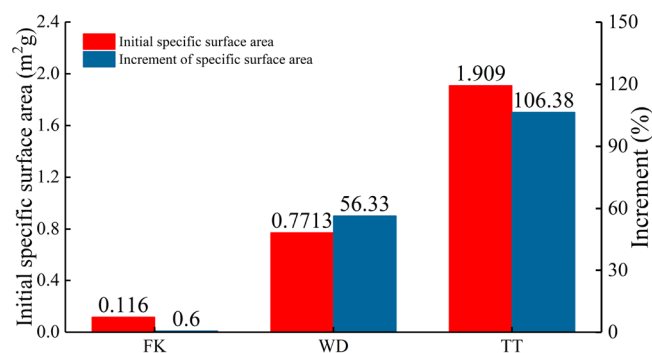


**Figure 15.** Histogram of specific surface area and increments. Samples FK and WD are dried intact samples; TT is a dried powdered sample.

sample will hinder the flow and adsorption of nitrogen. However, the LP-CO<sub>2</sub>GA data showed no significant increase in micropores PSD between dried and wetted samples after nitrogen injection (Figures 9 and 10), presumed as a result of capillary exclusion. It should be noted that the LP-N<sub>2</sub>GA, LP-CO<sub>2</sub>GA, and isothermal adsorption experiments also have gas adsorption processes, but due to the lower pressure and shorter time measured in experiments,<sup>18,43</sup> there will be no significant impact on the experimental results of nitrogen injection.

These PSD and adsorption capacity changes are of great significance to the stimulation of gas injection and the sequestration of carbon dioxide. Nitrogen injection also has an important practical significance for carbon dioxide geological storage. The swelling of coal caused by carbon dioxide adsorption will make injection difficult.<sup>2</sup> Pre-injection of nitrogen can improve the connectivity and adsorption capacity of reservoir pores and fractures and enhance carbon dioxide injection. The field result of the Ishikari coalfield demonstrates this potential.<sup>2</sup> Compared with the data for carbon dioxide injection either without or after nitrogen injection, the injection amount and injection rate of carbon dioxide are significantly increased due to the enhancement of permeability and adsorption capacity.<sup>2</sup> For the geological storage of carbon dioxide in deep undeveloped coal seams, the permeability of the coal reservoir is very low due to the large stress. In this case it is difficult to continuously and rapidly inject a large amount of carbon dioxide.<sup>42,44</sup> Thus, it is important to improve the injection rate and injection volume for carbon dioxide storage. In CBM production, hydraulic fracturing is commonly used to improve reservoir permeability. Conversely, for carbon dioxide storage, due to the strong heterogeneity of the coal reservoir, it is difficult to control the fracture distribution direction and fracture length caused by hydraulic fracturing.<sup>45</sup> Thus, nitrogen injection can pre-characterize the fracture system prior to carbon dioxide storage. For example, nitrogen injection before carbon dioxide injection can not only improve the injection rate of carbon dioxide, but also improve the storage capacity of carbon dioxide. Moreover, the adsorption capacity of nitrogen is significantly smaller than that of carbon dioxide. Even if nitrogen is adsorbed into the coal reservoir, it will be replaced by carbon dioxide.<sup>46,47</sup>

The research in this work is only based on six samples of highly volatile bituminous coal from three coal mines. The

nitrogen injection effect of other coal reservoirs with different coal rank and physical parameters needs further analysis and research.

## 5. CONCLUSIONS

In the current work, the characteristics of PSD and adsorption capacity of highly volatile bituminous coal after nitrogen injection are analyzed. HPMI, LP-N<sub>2</sub>GA, and LP-CO<sub>2</sub>GA were used to study changes in the PSD of the coal from before and after nitrogen injection, with LF-NMR and isothermal adsorption used to study the changes of adsorption capacity.

- (1) After nitrogen injection, the specific pore volume and specific surface area of macropores (>50 nm), mesopores (2–50 nm), and micropores (<2 nm) increased. The increase in specific surface area leads to an increase in the gas adsorption capacity, and the increase in micropore specific surface area plays an important role in the increase of the overall adsorption capacity.
- (2) With the increase or decrease in pore size, the effect of nitrogen exhibits no specific systematic pattern, although the larger the adsorption capacity, the larger the change in PSD.
- (3) Higher mineral content and a more heterogeneous distribution of macerals has a larger impact on the effect of nitrogen injection on coal pore and adsorption capacity. The presence of water impacts the effect of nitrogen injection on mesopores, but has little effect on micropores.

## ■ AUTHOR INFORMATION

### Corresponding Author

**Xuehai Fu** – Key Laboratory of Coalbed Methane Resources and Reservoir Formation Process, Ministry of Education, China University of Mining and Technology, Xuzhou, Jiangsu 221008, China; [orcid.org/0000-0002-6566-5148](https://orcid.org/0000-0002-6566-5148); Email: [fxuehai@cumt.edu.cn](mailto:fxuehai@cumt.edu.cn)

### Authors

**Junqiang Kang** – Key Laboratory of Coalbed Methane Resources and Reservoir Formation Process, Ministry of Education, China University of Mining and Technology, Xuzhou, Jiangsu 221008, China; Energy and Mineral Engineering, G3 Center and EMS Energy Institute, Pennsylvania State University, University Park, Pennsylvania 16801, United States

**Derek Elsworth** – Energy and Mineral Engineering, G3 Center and EMS Energy Institute, Pennsylvania State University, University Park, Pennsylvania 16801, United States

**Shun Liang** – School of Mines, Key Laboratory of Deep Coal Resource Mining, Ministry of Education of China, China University of Mining and Technology, Xuzhou 221116, China

Complete contact information is available at: <https://pubs.acs.org/10.1021/acs.energyfuels.0c01223>

### Notes

The authors declare no competing financial interest.

## ■ ACKNOWLEDGMENTS

The current work was supported by joint Ph.D. program of “double first rate” construction disciplines of CUMT.

## ■ REFERENCES

- (1) Reeves, S.; Oudinot, A. *The Tiffany Unit N<sub>2</sub>-ecbm Pilot: a Reservoir Modeling Study*; U.S. Department of Energy Topical Report; U.S. Department of Energy, 2004.
- (2) Shi, J.; Durucan, S.; Fujioka, M. A reservoir simulation study of co injection and n flooding at the ishikari coalfield co storage pilot project, japan. *Int. J. Greenhouse Gas Control* **2008**, *2*, 47–57.
- (3) Mazzotti, M.; Pini, R.; Storti, G. Enhanced coalbed methane recovery. *J. Supercrit. Fluids* **2009**, *47*, 619–627.
- (4) Pan, Z.; Connell, L. Modelling of anisotropic coal swelling and its impact on permeability behaviour for primary and enhanced coalbed methane recovery. *Int. J. Coal Geol.* **2011**, *85*, 257–267.
- (5) Wang, H.; Fu, X.; Jian, K.; Li, T.; Luo, P. Changes in coal pore structure and permeability during N<sub>2</sub> injection. *J. Nat. Gas Sci. Eng.* **2015**, *27*, 1234–1241.
- (6) Kang, J.; Fu, X.; Li, X.; Liang, S. Nitrogen injection to enhance methane and water production: An experimental study using the LF-NMR relaxation method. *Int. J. Coal Geol.* **2019**, *211*, 103228.
- (7) Kang, J.; Fu, X.; Liang, S.; Zhou, F.; Li, Y. Experimental study of changes in fractures and permeability during nitrogen injection and sealing of low-rank coal. *J. Nat. Gas Sci. Eng.* **2018**, *57*, 21–30.
- (8) Gathitu, B.; Chen, W.; McClure, M. Effects of coal interaction with supercritical CO<sub>2</sub>: physical structure. *Ind. Eng. Chem. Res.* **2009**, *48*, 5024–5034.
- (9) Liu, C.; Wang, G.; Sang, S.; Rudolph, V. Changes in pore structure of anthracite coal associated with CO<sub>2</sub> sequestration process. *Fuel* **2010**, *89*, 2665–2672.
- (10) Liu, J.; Yao, Y.; Liu, D.; Elsworth, D. Experimental evaluation of CO<sub>2</sub> enhanced recovery of adsorbed-gas from shale. *Int. J. Coal Geol.* **2017**, *179*, 211–218.
- (11) Sampath, K.; Perera, M.; Ranjith, P.; Li, D. Qualitative and quantitative evaluation of the alteration of micro-fracture characteristics of supercritical CO<sub>2</sub>-interacted coal. *J. Supercrit. Fluids* **2019**, *147*, 90–101.
- (12) Hou, P.; Gao, F.; Ju, Y.; Cheng, H.; Gao, Y.; Xue, Y.; Yang, Y. Changes in pore structure and permeability of low permeability coal under pulse gas fracturing. *J. Nat. Gas Sci. Eng.* **2016**, *34*, 1017–1026.
- (13) Moore, T. Coalbed methane: a review. *Int. J. Coal Geol.* **2012**, *101*, 36–81.
- (14) Zou, M.; Wei, S.; Huang, Z.; Lv, X.; Guo, B. Simulations on recoverability performances for a coalbed methane field in SE edge of Ordos basin, China. *Fuel* **2018**, *233*, 354–360.
- (15) Yao, Y.; Liu, D.; Che, Y.; Tang, D.; Tang, S.; Huang, W. Petrophysical characterization of coals by low-field nuclear magnetic resonance (NMR). *Fuel* **2010**, *89*, 1371–1380.
- (16) Wang, Y.; Zhu, Y.; Chen, S.; Li, W. Characteristics of the nanoscale pore structure in Northwestern Hunan shale gas reservoirs using field emission scanning electron microscopy, high-pressure mercury intrusion, and gas adsorption. *Energy Fuels* **2014**, *28*, 945–955.
- (17) Okolo, G.; Everson, R.; Neomagus, H.; Roberts, M.; Sakurovs, R. Comparing the porosity and surface areas of coal as measured by gas adsorption, mercury intrusion and saxs techniques. *Fuel* **2015**, *141*, 293–304.
- (18) Pan, J.; Lv, M.; Hou, Q.; Han, Y.; Wang, K. Coal microcrystalline structural changes related to methane adsorption/desorption. *Fuel* **2019**, *239*, 13–23.
- (19) Zheng, S.; Yao, Y.; Liu, D.; Cai, Y.; Liu, Y. Nuclear magnetic resonance surface relaxivity of coals. *Int. J. Coal Geol.* **2019**, *205*, 1–13.
- (20) ISO 17246: *Coal-Proximate Analysis*; International Organization for Standardization: Geneva, Switzerland, 2005.
- (21) ISO 7404-5: *Methods for the petrographic analysis of coals - part 5: method of determining microscopically the reflectance of vitrinite*; International Organization for Standardization: Geneva, Switzerland, 2009.
- (22) Niu, Q.; Pan, J.; Jin, Y.; Wang, H.; Li, M.; Ji, Z.; Wang, K.; Wang, Z. Fractal study of adsorption-pores in pulverized coals with various metamorphism degrees using N<sub>2</sub> adsorption, X-ray scattering and image analysis methods. *J. Pet. Sci. Eng.* **2019**, *176*, 584–593.
- (23) Li, X.; Hayashi, J. I.; Li, C. Z. FT-Raman spectroscopic study of the evolution of char structure during the pyrolysis of a Victorian brown coal. *Fuel* **2006**, *85*, 1700–1707.
- (24) Zhao, Y.; Fang, Q.; Wan, Z.; Yuan, Z.; Liang, W.; Meng, Q. Experimental investigation on correlation between permeability variation and pore structure during coal pyrolysis. *Transp. Porous Media* **2010**, *82*, 401–412.
- (25) Luo, P.; Zhong, N. The role of residual bitumen on the pore structure of organic-rich shales from low to over mature: Insight from shale and coal samples after the hydrous pyrolysis. *Int. J. Coal Geol.* **2020**, *226*, 103515.
- (26) Niu, Q.; Cao, L.; Sang, S.; Zhou, X.; Wang, Z. Anisotropic adsorption and permeability characteristics with injecting CO<sub>2</sub> in coal. *Energy Fuels* **2018**, *32*, 1979–1991.
- (27) Zheng, S.; Yao, Y.; Liu, D.; Cai, Y.; Liu, Y.; Li, X. Nuclear magnetic resonance T<sub>2</sub> cutoffs of coals: A novel method by multifractal analysis theory. *Fuel* **2019**, *241*, 715–724.
- (28) Yao, Y.; Liu, D.; Xie, S. Quantitative characterization of methane adsorption on coal using a low-field NMR relaxation method. *Int. J. Coal Geol.* **2014**, *131*, 32–40.
- (29) Ramirez, A.; Sierra, L.; Mesa, M.; Restrepo, J. Simulation of nitrogen adsorption-desorption isotherms. hysteresis as an effect of pore connectivity. *Chem. Eng. Sci.* **2005**, *60*, 4702–4708.
- (30) Nikom, K.; Nicholson, D. On the hysteresis loop and equilibrium transition in slit-shaped ink-bottle pores. *Adsorption* **2013**, *19*, 1273–1290.
- (31) Wang, F.; Yao, Y.; Wen, Z.; Sun, Q.; Yuan, X. Effect of water occurrences on methane adsorption capacity of coal: A comparison between bituminous coal and anthracite coal. *Fuel* **2020**, *266*, 117102.
- (32) Zheng, S.; Yao, Y.; Liu, D.; Cai, Y.; Liu, Y. Characterizations of full-scale pore size distribution, porosity and permeability of coals: A novel methodology by nuclear magnetic resonance and fractal analysis theory. *Int. J. Coal Geol.* **2018**, *196*, 148–158.
- (33) Yao, Y.; Liu, J.; Liu, D.; Chen, J.; Pan, Z. A new application of NMR in characterization of multiphase methane and adsorption capacity of shale. *Int. J. Coal Geol.* **2019**, *201*, 76–85.
- (34) Dawson, G.; Golding, S.; Esterle, J.; Massarotto, P. Occurrence of minerals within fractures and matrix of selected Bowen and Ruhr Basin coals. *Int. J. Coal Geol.* **2012**, *94*, 150–166.
- (35) Cai, Y.; Liu, D.; Pan, Z.; Yao, Y.; Li, J.; Qiu, Y. Pore structure and its impact on CH<sub>4</sub> adsorption capacity and flow capability of bituminous and subbituminous coals from northeast china. *Fuel* **2013**, *103*, 258–268.
- (36) Wang, Z.; Pan, J.; Hou, Q.; Yu, B.; Li, M.; Niu, Q. Anisotropic characteristics of low-rank coal fractures in the Fukang mining area, China. *Fuel* **2018**, *211*, 182–193.
- (37) Wei, M.; Liu, J.; Elsworth, D.; Li, S.; Zhou, F. Influence of gas adsorption induced non-uniform deformation on the evolution of coal permeability. *Int. J. Rock Mech Min* **2019**, *114*, 71–78.
- (38) Zhao, X.; Wang, J.; Mei, Y. Analytical Model of Wellbore Stability of Fractured Coal Seam Considering the Effect of Cleat Filler and Analysis of Influencing Factors. *Appl. Sci.* **2020**, *10*, 1169.
- (39) Massarotto, P.; Golding, S.; Bae, J.; Iyer, R.; Rudolph, V. Changes in reservoir properties from injection of supercritical CO<sub>2</sub> into coal seams - a laboratory study. *Int. J. Coal Geol.* **2010**, *82*, 269–279.
- (40) Gibbs, J. On the equilibrium of heterogeneous substances. *Am. J. Sci.* **1878**, *s3-16*, 300–320.
- (41) Griffith, A. The phenomena of rupture and flow in solids. *Philosophical Transactions of the Royal Society of London Series A, Containing Papers of a Mathematical or Physical Character* **1921**, *221*, 163–198.
- (42) Bachu, S.; Bonijoly, D.; Bradshaw, J.; Burruss, R.; Holloway, S.; Christensen, N.; Mathiassen, O. CO<sub>2</sub> storage capacity estimation: methodology and gaps. *Int. J. Greenhouse Gas Control* **2007**, *1*, 430–443.

(43) Zhang, D.; Cui, Y.; Liu, B.; Li, S.; Song, W.; Lin, W. Supercritical pure methane and CO<sub>2</sub> adsorption on various rank coals of China: experiments and modeling. *Energy Fuels* **2011**, *25*, 1891–1899.

(44) Botnen, L.; Fisher, D.; Dobroskok, A.; Bratton, T.; Greaves, K.; McLendon, T.; Steiner, G.; Sorensen, J.; Steadman, E.; Harju, J. Field test of CO<sub>2</sub> injection and storage in lignite coal seam in north dakota. *Energy Procedia* **2009**, *1*, 2013–2019.

(45) Wu, C.; Zhang, X.; Meng, W.; Zhou, L.; Wei, J. Physical simulation study on the hydraulic fracture propagation of coalbed methane well. *J. Appl. Geophys* **2018**, *150*, 244–253.

(46) Kelemen, S.; Kwiatek, L. Physical properties of selected block argonne premium bituminous coal related to CO<sub>2</sub>, CH<sub>4</sub>, and N<sub>2</sub> adsorption. *Int. J. Coal Geol.* **2009**, *77*, 2–9.

(47) Ottiger, S.; Pini, R.; Storti, G.; Mazzotti, M. Measuring and modeling the competitive adsorption of CO<sub>2</sub>, CH<sub>4</sub>, and N<sub>2</sub> on a dry coal. *Langmuir* **2008**, *24*, 9531–9540.